JOURNAL OF OPTOELECTRONICS AND ADVANCED MATERIALS Vol. 8, No. 5, October 2006, p. 1672 - 1678

Invited Paper

Peculiarities and potentialities of ultra-short pulsed laser deposition for the production of magnetic nanogranular films

L. LANOTTE[a*], G. AUSANIO[a], A. C. BARONE[a], C. HISON[b], V. IANNOTTI[a], S. AMORUSO[c], R. BRUZZESE[c], M. VITIELLO[c], M. D'INCAU[d], P. SCARDI[d]

[a]*Coherentia CNR-INFM and Dipartimento di Scienze Fisiche, Università degli Studi di Napoli "Federico II", P.le V. Tecchio 80, I-80125 Napoli, Italy*

[b]*Coherentia CNR-INFM and Dipartimento di Ingegneria dei Materiali e della Produzione, Università degli Studi di Napoli "Federico II", Piazzale V. Tecchio 80, I-80125 Napoli, Italy*

[c]*Coherentia CNR-INFM and Dipartimento di Scienze Fisiche, Università degli Studi di Napoli "Federico II", Via Cintia, I-80126 Napoli, Italy*

[d]*Materials Engineering&Industrial Technologies Dep., Trento University , Via Mesiano 77, -38050 Trento, Italy*

Pulsed laser deposition is a technique used since twenty years ago for the production of nanoparticles films. Laser pulses with a duration in the femtosecond, picosecond and nanosecond range have been employed for material processing as well as for ablation and deposition of semiconductors, superconductive materials, ceramics, magnetic layers and multilayers. Recently, results on the ultra-short pulsed laser deposition (uPLD) revealed this technique as particularly interesting for the deposition of magnetic nanogranular films. This review deals with the innovative findings and the potential developments related to the use of uPLD. The following points are addressed: first, the peculiar shape and orientation of the nanoparticles in the films obtained by the uPLD technique; second, the capability of uPLD to reproduce the stoichiometry in target material in the deposited film; third, the possibility to produce nanogranular amorphous film from polycrystalline target; fourth, the potentiality of uPLD in tailoring the magnetic softness of the film by means of a co-deposition of hard and soft magnetic nanoparticles. Finally, we briefly discuss the potential applications of the uPLD in the production of composite nanogranular films with interesting performances for improved magnetostrictive and magnetoresisitive micro-devices.

(Received September 5, 2006; accepted September 13, 2006)

Keywords: Magnetic nanogranular films, Pulsed laser deposition, Fine particles structure

1. Introduction

In the last three decades, increasing research efforts have been devoted to magnetic nanoparticles films by virtue of their peculiar properties making them very suitable for many technological applications, among which magnetic recording [1,2], high-frequency field-amplifying systems [3], magnetoelastic and magnetotransport active components for micro-devices [4,5], high coercive magnets [6], etc.

Among the several techniques used to prepare nanostructured films, the ablation by means of nanosecond laser pulses (pulsed laser deposition (PLD)) [7] is one of the most effective, in particular because it is fast and it preserves the original stoichiometry of the target material, strongly reducing the inclusion of impurities [8, 9]. On the other hand, laser ablation is a complex process which is not yet fully understood particularly for what concerns the mechanisms involved in the laser-matter interaction process for different laser pulse durations going from ns to fs time scales [10, 11].

Since three years ago we have focused our investigations on the merits of pulsed laser deposition with ultrashort pulses characterized by duration of some fraction of a picosecond, a technique dubbed ultrashort PLD (uPLD). The use of a shorter interaction time between the laser pulse and the target material can significantly change the characteristics of the deposited films with respect to those obtained by standard PLD, providing novel potentialities for improving and widening the field of application of nanogranular films [12-15].

This paper reviews the state of the art of uPLD technique, presenting its potentialities for the development of magnetic nanoparticles films. In particular, the following peculiar characteristics of the uPLD are pointed out:

- the process of nanoparticles generation and film deposition is different from the case of standard PLD;
- the nanoparticles constituting the film are characterized by a peculiar shape and orientation;
- for complex, multicomponent materials, the target stoichiometry is maintained in the deposited films;

- highly disordered nanogranular films can be obtained even starting from a crystalline target;
- co-deposition of different materials with soft and hard magnetic properties can be performed so that the magnetic characteristics of the obtained films are the average of the single component magnetic responses, resulting from the exchange coupling interaction among the nanoparticles.

2. Experimental

The schematic representation of the uPLD deposition process is shown in Fig. 1. The laser radiation is focused onto the target surface at an angle of 45°. The target is mounted on a rotating holder, to minimize the pit formation, in a vacuum chamber at a residual pressure of 10^{-5} Pa. Isolated nanoparticles (for deposition time shorter than 10 minutes) or nanogranular thin films (for longer deposition times) are deposited onto a suitable substrate hold parallel to the target at about 30 mm distance, and at room temperature. The target can be an elemental or multi-component material. Moreover, co-deposition of two or more materials, in nanoparticles form, can be performed by using an ablation target formed by different materials (see Fig. 1, e.g.). In this case, the volume fraction of each material in the deposited films is defined by the ablation rate and the permanence time of the laser beam on each section of the target (at a fixed target rotation velocity).

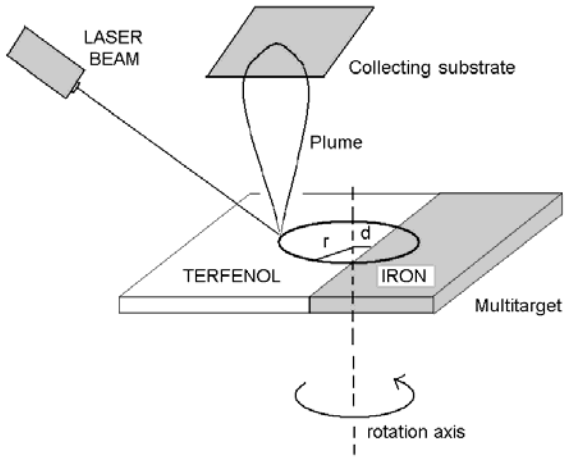

Fig. 1. Schematic representation of the uPLD in the case of a co-deposition of a target made by two different materials.

The experiments were performed by using different laser sources, whose characteristics are summarized in Table 1, in order to study the influence of the radiation wavelength, intensity and repetition rate on the properties of deposited film. The laser pulse energy was changed by means of calibrated attenuating plates, while Pockel's cells were used to decrease the laser repetition rate.

Table 1. Laser sources characteristics.

Source type	Pulse energy (mJ)	Wavelength (nm)	Pulse duration FWMH (fs)	Frequency (Hz)	Residual pressure (Pa)	Spot size (cm^2)
Amplified solid state Ti:Sapphire	0.5÷1	780	120	10÷1000	10^{-5}	2×10^{-4}
Chirped pulse amplification based Nd:Glass	0.5÷4	1055	850	1÷33	10^{-5}	$2\div7\times10^{-4}$
Second harmonic generation pulse compression Nd:Glass	0.2÷1.3	527	250÷300	1÷33	10^{-5}	2×10^{-4}

Nanoparticle dynamics in the plume produced by ultrashort laser ablation process was investigated by Optical Emission Spectroscopy (OES) and Fast Photography techniques [16].

The morphology of the isolated particles, as well as of the nanogranular layers, was studied by an Atomic Force Microscope (AFM, Nanoscope IIIa Digital Instruments) operating in tapping mode. AFM images allowed analyzing the surface topography with indication also on the profiles orthogonal to the surface plane. Programs for the statistics of the nanoparticle size were implemented in the elaboration software of the AFM data.

X-Ray Diffraction (XRD) was used for the structural analysis of the target and of the deposited films, while their chemical composition was determined by micro Energy Dispersive X-Ray Spectroscopy (mEDXS).

The first magnetization curves and magnetic hysteresis cycles in the deposited films plane were drawn by means of a Vibrating Sample Magnetometer (VSM, Maglab 9T Oxford Instruments), calculating, after reiterated experiments, the typical values of coercivity, saturation magnetizing field, remanence and saturation magnetization.

3. uPLD technique peculiarities

3.1. Mechanism of nanoparticles production

In the standard PLD, pulse durations of the order of tens nanosecond leads to the heating of a thick region (typically of few microns) below the target surface, as a consequence of the laser-matter interaction and thermal

conduction into the target material. The temperature achieved in the layer under the surface reaches values high enough to produce its evaporation and the consequent ejection of atoms and aggregates characterized by high velocities ($\approx 10^3$-10^4 m/s) in the direction perpendicular to the target surface, which finally forms an ablation plume.

Atoms and ions collisions near the deposition substrate determine the formation of primary nucleation centers for the subsequent nanoparticles growing process. Therefore, the residual pressure in the deposition chamber and the nature of the substrate play a determinant role in the nanoparticles formation [17, 18] and continuous films can often be obtained [19].

The use of laser pulses with a duration shorter than few picosecond in ultrashort laser ablation, involves a completely different process of nanoparticles formation. In fact, laser radiation absorption and heating affect only a surface layer with a thickness of the order the material skin depth and occur on such a short time scale that the heating process can be considered nearly isochoric. The high increase in temperature is accompanied by an enormous pressure gradient [20, 21] within the heated layer. Then, a quasi-adiabatic expansion of this layer occurs. During this phase, the surface material can be driven into the metastable region of the phase diagram, resulting in the emission of nanoparticles via phase explosion, fragmentation or spinodal decomposition, as illustrated in recent theoretical analysis of the process [21, 22].

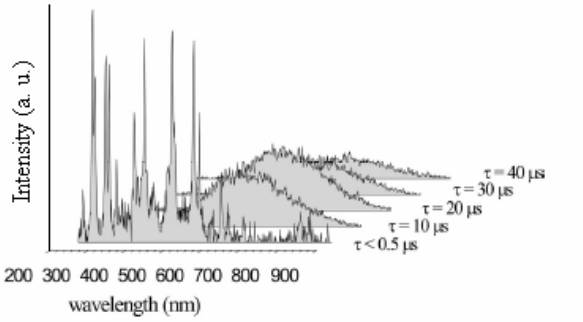

Fig. 2. Typical emission spectra of the plume for different time delays, τ, (time passed from the laser pulse incidence on the target), at a distance of 1 mm from the target, characteristic to the femtosecond ablation of mono- and multi-component target materials. The figure refers to the ablation of an Au target (laser fluence: 0.6 Jcm^{-2}, wavelength: 780 nm, repetition rate: 1kHz).

An experimental proof that nano-sized fragments are present in a significant amount in the ablation plume is given by optical emission spectroscopy analysis of the ablated material. As an example, Fig. 2 show typical emission spectra of the plume produced during laser ablation of an Au target for different time delays after the end of the laser pulse [14].

The broad continuum emission detected for $\tau > 5\mu s$, at a distance of 1 mm from the target, demonstrates that a number of nanosized particle are effectively emitted. Moreover, when the removed matter is collected onto a substrate, it was experimentally found that particles with a mean size between 5 and 20 nm compose the plume, as can be seen in Fig. 3. The figure shows typical isolated nanoparticles deposited onto a mica substrate, after a short irradiation time (some minutes) for which less than one layer of material is deposited. The statistical values of the average mean radius, R_m, and major radius, R_{max}, of the oblate shape particles, for different target materials and laser intensities, have been found are not much different for the various materials (metal, semi-conductor, mono and multi-component target) and the standard deviations, as well as the size distribution dispersions, are also very similar [14]. This indicates that the nanoparticles are a peculiar product of the uPLD process in the above mentioned intensity range, weakly depending on the specific target material.

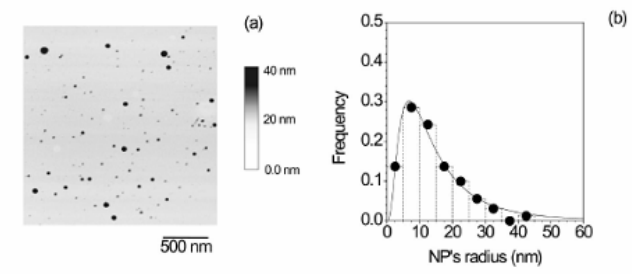

Fig. 3. (a) AFM image of Ag nanoparticles deposited in a high vacuum (≈10^{-5} Pa) onto a mica substrate. (b) Size histogram of the deposited Ag nanoparticles. The solid curve is a guide to the eye.

3.2. Morphology of the deposited particles

For a more accurate analysis of the deposited particles morphology, not only the average particles radius determined from the AFM images of a surface parallel to the substrate plane, but also the particles profiles in different cross sections orthogonal to the substrate plane must be considered. This deeper investigation shows clearly that all the deposited particles present a typical shape, very similar to an oblate ellipsoid. Moreover, the ellipsoidal particles have the major cross section preferentially oriented in a plane parallel to the deposition substrate. This systematic finding is in agreement with other results showing that the nanoparticles deposited onto the substrate derive from material fragments already present in the plume. In fact, if we assume that the particles arrive already formed on the substrate, their shape can be explained as an effect of the impact, occurring when their temperature is about 1000°C. The hot material fragments from the plume arrive on the substrate at high velocities, along a propagation axis, X, as shown in Fig. 4. Since the particles are in fluid phase, the compressive stress along X axis, determined by the impact with the substrate, can produce the characteristic flattening of the shape, conserved also after solidification (Fig. 4).

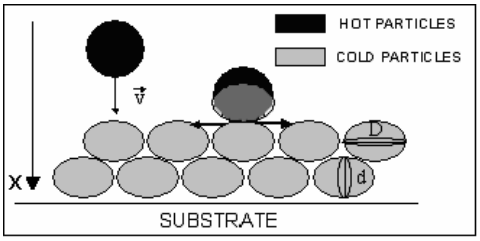

Fig. 4. Mechanism of particle deposition which determine s their peculiar oblate ellipsoidal shape.

The peculiar oblate ellipsoidal shape can be distinguished very well in the AFM images of the isolated nanoparticles obtained after some deposition minutes (Fig. 5, a and c). This specific shape is maintained also in the case of a continuous layer obtained for longer deposition times (Fig. 5, b and d).

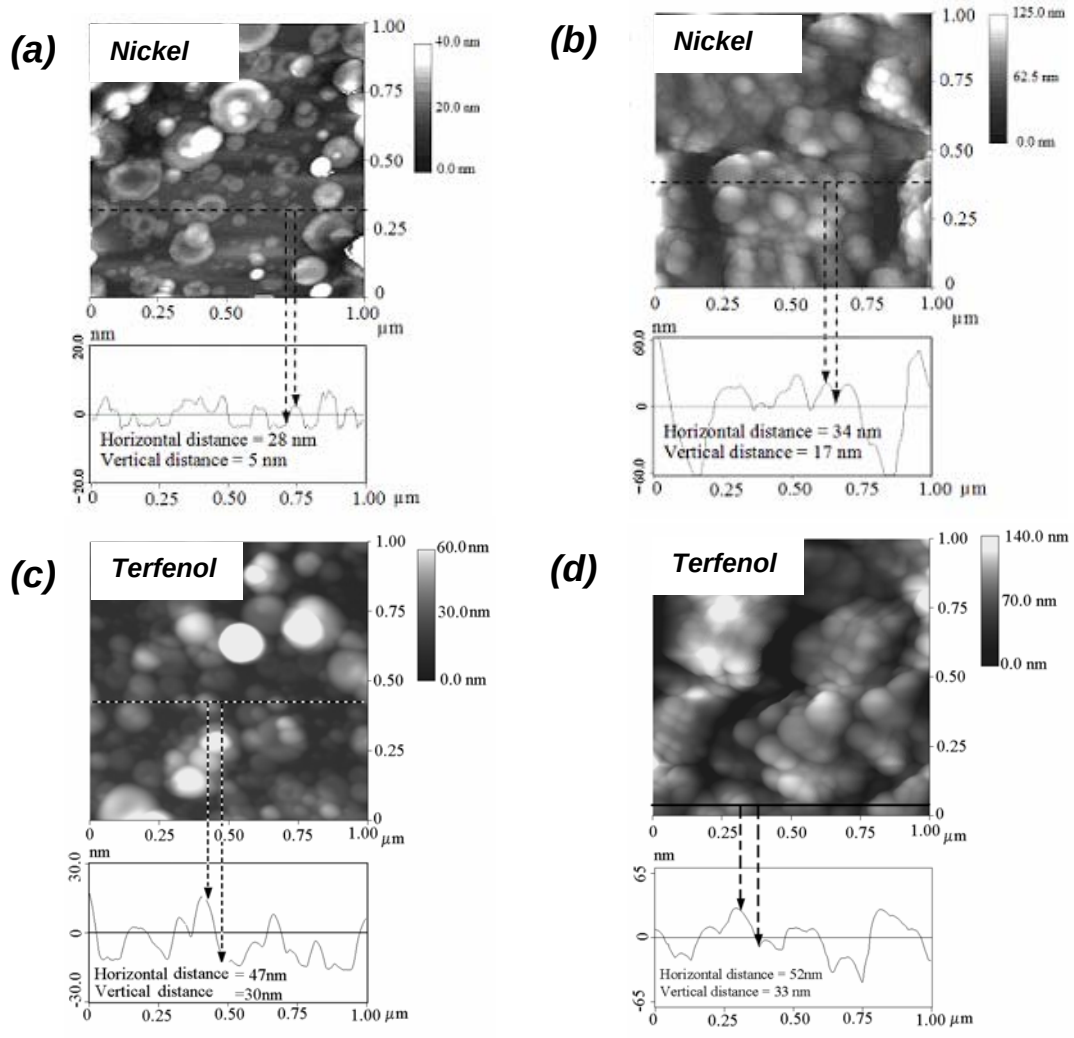

Fig. 5. AFM images of the uPLD film surface and the corresponding cross section profiles at an early formation stage: 360 s in the cases (a) and (c) and after long deposition times: 3600 s in the cases (b) and (d).

The AFM data show also that the particles eccentricity decreases with the complete film formation. This is obviously related to the fact that in the film case, only the first layer of particles is deposited onto the substrate surface, while the subsequent layers form onto the nanogranular film already grown, therefore the solidification is governed by different thermal coefficients.

By comparing the surface AFM images and the corresponding profiles orthogonal to the substrate, it is possible to make a statistic analysis of both major, D, and minor, d, cross section diameters of the deposited nanoparticles.

The average values of the shape parameters, D and d, and of the particle eccentricity for different target materials and laser intensities are reported in Table 2. It can be seen that the ellipsoidal shape is standard for both mono- and multi-component materials. In particular for metals, a general increase in eccentricity is obtained by increasing the laser pulse intensity.

Table 2. Particles shape characteristics for different target materials and deposition parameters: S = film thickness, D = particles major diameter, d = particles minor diameter, D/d = particle eccentricity.

Sample Code	Laser pulse duration/wavelenght	Intensity (W/cm^2)	Deposition time (s)	S (nm)	D (nm)	d (nm)	D/d
7Ni	0.85 ps/1055 nm	3.5×10^{11}	3600	100	42	41	1.0
8Ni	0.85 ps/ 1055 nm	7.1×10^{11}	3600	180	47	34	1.4
9Ni	0.85 ps/1055 nm	1.0×10^{12}	3600	1200	55	40	1.4
10Ni	0.30 ps/527 nm	1.3×10^{12}	3600	650	43	13	3.3
11Ni	0.30 ps/527 nm	2.5×10^{12}	3600	350	51	14	3.6
12Ni	0.30 ps/527 nm	3.7×10^{12}	3600	900	65	16	4.1
7Si	0.85 ps/1055 nm	7.3×10^{11}	3600	400	39	24	1.6
8Si	0.30 ps/527 nm	1.2×10^{12}	3600	400	55	14	3.9
9Si	0.30 ps/527 nm	2.1×10^{12}	3600	500	99	15	6.6
10Si	0.30 ps/527 nm	3.7×10^{12}	3600	1000	114	24	4.8
$Tb_{0.3}Dy_{0.7}Fe_2$	0.30 ps/527 nm	3.7×10^{12}	3600	700	79	24	3.3
Fe	0.30 ps/527 nm	3.7×10^{12}	3600	2000	86	40	2.2

3.3. Reproduction of the target material stoichiometry

Another important characteristic of the uPLD technique is the good reproducibility of the target material chemical composition in the deposited thin film. This is particularly useful when multi-component target are employed and a precise fraction of nanoparticles, having the same stoichiometry of the target material, are desired in the deposited film. An example referred to the case of Iron and $Tb_{0.3}Dy_{0.7}Fe_2$ co-deposition is reported in Table 3 which reports: 1) the volume fraction of the two components as expected from the permanence time of the laser beam on each target region, and from their relative deposition efficiency; 2) the atomic fractions of each element in the deposited film as experimentally determined by micro-EDXS; 3) the corresponding expected values of the atomic fractions in the hypothesis that the deposited particles reproduce the stoichiometry of the target materials. All the fraction values are given normalizing to 1 the total fractions of Tb+Dy.

Considering a 10% experimental error on the parameters from which the expected values are obtained, the agreement between expected and the experimental values is satisfactory. This point is of particular relevance, since the retention of the stoichiometry is demonstrated not only in the case of a single, multielemental, target as Terfenol but also in the case of co-deposition of two different material.

Table 3. Expected (calculated) and the experimental atomic fractions of the target components in the films deposited by uPLD from a multi-components target made of $Tb_{0.3}Dy_{0.7}Fe_2$ (Terfenol-D) and pure Fe, in the percentages shown in the first column.

Expected volume fraction	Experimental atomic fractions			Expected atomic fractions		
	Tb	Fe	Dy	Tb	Fe	Dy
$Terfenol_{100}$	0.31	1.91	0.69	0.3	2.0	0.7
$Terfenol_{85}Fe_{15}$	0.30	2.87	0.70	0.3	2.9	0.7
$Terfenol_{70}Fe_{30}$	0.26	3.79	0.74	0.3	4.0	0.7
$Terfenol_{60}Fe_{40}$	0.24	5.78	0.76	0.3	5.8	0.7

3.4. Structure of thin films deposited from a crystalline target material

The shorter time for the energy transfer from the laser radiation to the target surface in the case of femtosecond pulses, as compared to the nanosecond ones, not only changes the formation process of the nanoparticles, as described in section 3.1, but also increases the temperature of nano-fragments expulsed from the target. Subsequently, their temperature at the impact with the substrate is higher [14] and they are subjected to a rapid cooling during the solidification process.

In the case of multicomponent nanoparticles, the high temperature/time gradients favor the formation of a disordered structure in the quasi-liquid nano-fragments ejected from the target, and the preservation of an amorphous state during the rapid solidification on the substrate (in a way similar to what happens during the rapid quenching from the melt of the metallic alloys [23, 24]). A proof of this process is provided by the study of the Terfenol-D films obtained by uPLD. In fact, unlike thin films produced by standard PLD X-ray diffraction does not show a crystalline pattern for Terfenol-D films produced by uPLD. The comparison between the

crystalline pattern of the target material and the pattern of the deposited film is shown in Fig. 6.

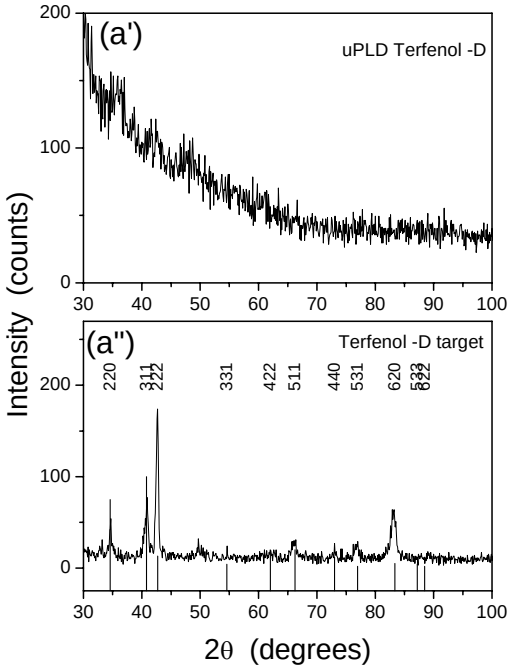

Fig. 6. XRD data showing the structureless pattern of the film obtained by femtosecond laser ablation (a') compared with the crystalline $Tb_{0.3}Dy_{0.7}Fe_2$ target (a'').

3.5. Magnetic properties of a nanogranular films obtained by co-deposition of different composition nanoparticles

Nanogranular magnetic films made of two or more components, as for example Fe + Ag, Co + Pt, Co + Cu, Ni + Fe, TbDyFe + Fe, are assuming increasing importance in the field of micro and nano-technology, due to their magnetoresistive, magnetostrictive and transport properties.

Theoretically, in specific conditions, exchange magnetic interactions can be activated among the nanoparticles determining new, interesting magnetic performances derived from the mixing of the components magnetic properties. Similar effects have already been produced in multilayers [25].

We will show that some first steps in this direction have been taken by exploiting the potentialities of the uPLD technique. The reported results were obtained by co-deposition of Fe and $Tb_{0.3}Dy_{0.7}Fe_2$ (Terfenol-D), using a multi-target as that shown in Fig. 1. The first magnetization curves for different iron contents and the corresponding magnetization parameters are reported in Fig. 7 and Table 4, respectively.

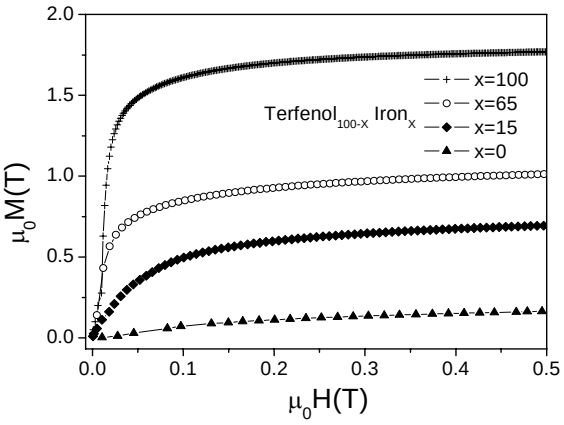

Fig. 7. First magnetization curves of the nanogranular films obtained by co-deposition of Fe and $Tb_{0.3}Dy_{0.7}Fe_2$ (Terfenol-D) by uPLD, for different Fe contents.

The increase of iron content gives obviously a softer magnetic response. It is very interesting that the macroscopic magnetization curves are not simply the sum of two separate responses, as expected if each magnetic component behaved separately. The curves appear indeed as the response of a single magnetic material originated from the mixture of the two components. This is confirmed by data presented in Table 4, where the experimental values are compared with those expected from the weighted mean of each component, shown in parentheses. In particular the coercive field and the saturation magnetization practically behave as deduced from changing of the iron content, while the iron seams to facilitate both saturation and remanence more than that expected from its percentage increase. All this leads to the conclusion that exchange interactions are effective in the nanogranular composite films.

Table 4. Magnetic characteristics of the nanogranular films obtained by co-deposition of Fe and $Tb_{0.3}Dy_{0.7}Fe_2$ (Terfenol-D) by uPLD, for different Fe contents.

Sample composition in volume fractions	Coercive field x μ_o (10^{-3} T)	Saturation field x μ_o (10^{-2} T)	Saturation magnetization x μ_o (T)	Remanence ratio
	Room temp.	Room temp.	Room temp.	Room temp.
$Terfenol_{100}$	43	170	0.29	0.08
$Terfenol_{85}Fe_{15}$	40 (38)	108 (147)	0.66 (0.52)	0.33 (0.15)
$Terfenol_{65}Fe_{35}$	30 (32)	77 (116)	0.88 (0.83)	0.38 (0.25)
$Terfenol_{35}Fe_{65}$	25 (22)	30 (70)	1.05 (1.29)	0.64 (0.40)
Fe_{100}	11	16	1.83	0.57

4. Conclusions and future trends

The ultra-short pulsed laser deposition is a practical route to produce nanogranular films of different magnetic materials (mono- and multi-component), made of nanoparticles with oblate ellipsoidal shape of controllable eccentricity, ranging from 1 to 10, major diameter of 40-100 nm and minor diameter as small as ≈10 nm. The ellipsoidal particles composing the deposited films are characterized by a common orientation of the major cross section parallel to the substrate plane.

The magnetic properties of the nanogranular films can be tailored by mixing nanoparticles of different magnetic materials.

Generally, the uPLD nanoparticles have crystalline structure, but in the case of complex compositions they can be obtained in disordered state more easily than by using standard PLD.

Taking into consideration all the features of the uPLD technique used for the preparation of nanogranular thin films, there are two very promising future trends:

1. production of oblate ellipsoidal shape nanoparticles with a thickness lower than 10 nm, by the improvement of the deposition technique. This possibility, together with the capability of co-depositing different material nanoparticles, can be the basis for the production of composite thin films made of a mixture of: semi-conductive and conductive nanoparticles, magnetic and non-magnetic nanoparticles (e.g. Si-Ni, Fe-Ag and Co-Au) characterized by Giant Hall effect or Giant Magnetoresistive effects similar to those occurring in multi-layers, but characterized by different interaction and anisotropies.

2. production of thin films exhibiting high magnetoelastic deformations activated by very low external fields, for application in cantilever devices, micro-sensors and micro-actuators. This objective can be pursued by continuing the study of nanogranular composite films made of mixtures of soft magnetic and high magnetostrictive particles.

Aknowledgements

We are grateful to the Italian MIUR for supporting this research in the frame of the project PRIN'05 *Production, characterization and modeling of nanogranular films with innovations in the magnetic, magnetoresistive or magnetostrictive properties.*

References

[1] A. A. Novakova, V. Yu. Lanchinskaya, A. V. Volkov, T. S. Gendler, T. Yu. Kiseleva, M. A. Moskvina, S. B. Zezin, J. Magn. Magn. Mater. **258**, 354 (2003).
[2] J. I. Martín, J. Nogués, Kai. Liu, J. L. Vicent, I. K. Schuller, J. Magn. Magn. Mater. **256**, 449 (2003).
[3] L. Lanotte, V. Iannotti, J. Appl. Phys. **78**, 3531 (1995).
[4] J. C. Sohn, D. J. Byun, S. H. Lim, J. Magn. Magn. Mater. 272-276, 1500 (2004).
[5] A. V. Svalov, P. A. Savin, G. V. Kurlyandskaya, J. Gutiérrez, J. M. Barandiarán, V. O. Vas'kovskiy, IEEE Trans. Magn. **38,** 2782 (2002).
[6] A. Singh, R. Tamm, V. Neu, S. Fahler, C.-G. Oertel, W. Skrotzki, L. Schultz, B. Holzapfel, J. Appl. Phys. **97**, 093902 (2005).
[7] T. J. Jackson, S.B. Palmer, J. Phys. D: Appl. Phys. **27**, 1581 (1994).
[8] D. Chrisey, G. K. Hubler (Eds.), Pulsed Laser Deposition of Thin Films, Wiley-Interscience, New York (1994).
[9] H. Sankur, J.T. Cheung, Appl. Phys. A **47**, 271 (1988).
[10] B. N. Chichkov, C. Momma, S. Nolte, F. Von Alvensleben, A. Tünnermann, Appl. Phys. A **63**, 109 (1996).
[11] A. V. Gusarov, I. Smurov, J. Appl. Phys. **97**, 014307 (2005).
[12] S. Amoruso, R. Bruzzese, N. Spinelli, R. Velotta, M. Vitiello, X. Wang, G. Ausanio, V. Iannotti, L. Lanotte, Appl. Phys. Lett. **84**, 4502 (2004).
[13] G. Ausanio, A.C. Barone, V. Iannotti, L. Lanotte, S. Amoruso, R. Bruzzese, M. Vitello, Appl. Phys. Lett. **85**, 4103 (2004).
[14] S. Amoruso, G. Ausanio, R. Bruzzese, M. Vitello, X. Wang, Phys. Rev. B **71**, 033406 (2005).
[15] S. Amoruso, G. Ausanio, C. de Lisio, V. Iannotti, M. Vitiello, X. Wang, L. Lanotte, Appl. Surf. Sci. **247**, 71 (2005).
[16] S. Amoruso, G. Ausanio, A. C. Barone, R. Bruzzese, L. Gragnaniello, M. Vitello, X. Wang, J. Phys. B: At. Mol. Opt. Phys. **38**, L329(2005).
[17] Q. Li, T. Sasaki, N. Koshizaki, Appl. Phys. A **69**, 115 (1999).
[18] S. R. Shinde, S. D. Kulkarni, A. G. Banpurkar, R. Nawathey-Dixit, S. K. Date, S. B. Ogale, J. Appl. Phys. **88**, 1566 (2000).
[19] G. V. Kurlyandskaya, J. M. Barandiarán, P. Mínguez, L. Elbaile, Nanotechnology **14**, 1246 (2003).
[20] P. Lorazo, L. J. Lewis, M. Meunier, Phys. Rev. Lett. **91**, 225502 (2003).
[21] S. Eliezer, N. Eliaz, E. Grossman, D. Fisher, I. Gouzman, Z. Henis, S. Pecker, Y. Horovitz, M. Fraenkel, S. Maman, Y. Lereah, Phys. Rev. B **69**, 144119 (2004).
[22] F. Vidal, T.W. Johnston, S. Laville, O. Barthélemy, M. Chaker, B. Le Drogoff, J. Margot, M. Sabsabi, Phys. Rev. Lett. **86**, 2573 (2001).
[23] L. Lovas, E. Kisdi-Koszo, L. Potocky, L. Novak, Journal of Materials Science **22,** 1535 (1987).
[24] M. Yagi, T. Sawa, IEEE Trans. Magn. **26**, 1409(1990).
[25] H. D. Chopra, M. R. Sullivan, A. Ludwig, E. Quandt, Phys. Rev. B **72**, 054415 (2005).

* Corresponding author: Lanotte@na.infn.it